Advances in Water Resources 45 (2012) 37–50

Contents lists available at SciVerse ScienceDirect

Advances in Water Resources

journal homepage: www.elsevier.com/locate/advwatres

The global space–time cascade structure of precipitation: Satellites, gridded gauges and reanalyses

S. Lovejoy [a,b,*], J. Pinel [a], D. Schertzer [c]

[a] Physics, McGill University, 3600 University St., Montreal, Quebec, Canada
[b] GEOTOP, UQAM, CP 8888, Succ. Centre Ville, Montreal, Quebec, Canada H3C 3P8
[c] LEESU, École des Ponts ParisTech, Université Paris-Est, 6-8 Av. B. Pascal, 77455 Marne-la-Vallée Cedex 2, France

ARTICLE INFO

Article history:
Available online 17 April 2012

Keywords:
Precipitation
Cascades
Fractals
Multifractals
Scaling
Disaggregation

ABSTRACT

Cascades have been used as models of precipitation for nearly 25 years yet many basic questions remain unanswered and most applications have been to small or to regional scales. In this paper we revisit some of these issues and present an inter comparison of four global scale data sets each with exceptional characteristics: the hourly (and ≈200 km) resolution Climate Prediction Center (CPC) gridded precipitation over the continental US, the three hourly global ECMWF reanalysis stratiform precipitation product at 1.5° resolution, the six hourly Twentieth Century reanalysis at 2° (1871–2008) and an analysis of 5300 orbits (1 year) of the Tropical Rainfall Measuring Mission (TRMM) satellite rainfall over ±40° latitude. The data were analysed zonally, meridionally and in time. Each showed cascade structures; in space up to planetary scales and in time up to 5–10 days. For each we estimated the moment scaling exponent ($K(q)$) as well as its characterisation near the mean (C_1) and the effective outer cascade scales. The comparison of the cascade structures in different directions indicate that although anomalies remain, they are relatively isotropic in (horizontal) space–time. For any given direction, the comparison of the different products indicates very similar but not identical scaling properties. In order to be properly inter calibrated at more than a unique resolution, the different products must have the same exponents and outer scales so that - while the similarities are encouraging – the remaining anomalies point to needed improvements in techniques for estimating areal rainfall. Our main conclusion is that the rain rate biases introduced by the measurement techniques are larger than the deviations from perfect log–log linearity (scaling) so that multifractal models will be needed for improving space–time precipitation measurements.

Our analyses clarify various fundamental issues. For example, the CPC data show that at "weather" scales smaller than ≈2 days in time; $H = 0.17 \pm 0.11$ so that rain is apparently not the direct product of a cascade process (which would have $H = 0$). Similarly, for the low frequency weather regime (scales >≈2 weeks) we find $H \approx -0.42$ so that fluctuations tend to decrease rather than increase with scale and display long range statistical dependencies. Finally, we find power law probability tails with exponent $q_D \approx 3$ so that the orders of singularity are apparently not bounded, ruling out several model types including microcanonical and log-Poisson models.

1. Introduction

1.1. Theoretical considerations

Precipitation is highly significant not only for meteorology where it plays a key role in the earth's energy and water budget, but also in hydrology. Yet it has a number of peculiarities making it somewhat different from most other atmospheric variables. First, from the empirical standpoint, the problem of estimating spatial (i.e. areal) rain rate fields – whether from (typically sparse) in situ networks of gauges, or from remote sensing (especially radar reflectivities) – is still not completely resolved. Strictly speaking – due to the resolution dependence associated with the intermittency – this could also be said of any of the other standard techniques used to produce smooth (gridded) fields from any in situ meteorological data (such as Kriging, optimal interpolation or 3D or 4D var); however, since rain is much more intermittent than the other fields this resolution effect is much stronger and more difficult to ignore. Indeed a main focus of this study is precisely to highlight the differences and similarities between

* Corresponding author at: Physics, McGill University, 3600 University St., Montreal, Quebec, Canada. Tel.: +1 514 398 6537.
E-mail address: lovejoy@physics.mcgill.ca (S. Lovejoy).

0309-1708/$ - see front matter © 2012 Elsevier Ltd. All rights reserved.
http://dx.doi.org/10.1016/j.advwatres.2012.03.024

precipitation and the standard meteorological state variables. Second, unlike the latter, rain intermittency probably has a significant "on/off" component: it is apparently zero at most times and places; yet even the exact definition of the (nonzero) "support" – the distinction between rain and no rain – is quite ad hoc, typically depending on the sensitivity of the instrument or the application area. It is possible that the on/off intermittency might be a threshold type effect in which case it is not scaling at all; the scale at which the threshold is introduced breaks the scaling. The possibility – even likelihood – that instrumental sensitivity introduces important artefacts can be surmised from the fact that minimum detectable rain rates (from remote or in situ techniques) are typically of the same order or larger (sometimes much larger) than the climatological mean rain rate (below – according to the ECMWF reanalysis – the global mean is ≈0.126 mm/hr). Indeed such threshold – induced scale breaks may explain many of the claims of breaks in the literature. Finally, from a modelling viewpoint, there are no theoretically "clean" ways to represent the rain rate in the same way as the main state variables – i.e. as coupled nonlinear partial differential equations. This forces precipitation modellers to resort to strong, largely ad hoc "parametrizations".

The idea of scaling in rain – especially in the hydrology literature – goes back at to least the study of streamflow time series [1]; it includes early contributions on long range statistical dependencies and extremes (essentially fractional Brownian motion and Levy processes, [2]), and also the wide range spatial scaling of rain [3]. The scaling idea also played a key role in the development of multifractals and for testing multiplicative cascades: an early review in rain already included over fifty references [4]. As scaling and cascade notions were increasingly applied to rain, a series of issues surfaced; some were related to the cascades themselves, whereas others concerned their relations to the multifractals they generate and to real world applications.

Before applying cascade models to rain we must first ask an apparently simple question: is the rainrate field itself the direct outcome of a cascade process or is it only driven/forced by a turbulent cascade generated flux? Certainly, the answer is not self-evident since in the usual meteorological cascades associated with the various state variables - the latter are only indirectly related to the underlying turbulent fluxes. Since multiplicative cascades conserve (on average) the turbulent fluxes from one scale to the next, the degree of (scale by scale) nonconservation needs to be determined, the conservation exponent H quantifies this (the symbol "H" is in honour of Hurst, but it is not the same as the "Hurst" exponent). For a pure multiplicative cascade, $H = 0$, if $H > 0$ then fluctuations tend to increase with scale, when $H < 0$, they tend to decrease with scale (see the next section and see Section 4 for the use of wavelets to quantify this). For example, in Kolmogorov three dimensional isotropic turbulence, the cascade is of energy flux which mathematically conserved scale by scale by the nonlinear dynamical terms; however, the observable wind field has an extra linear contribution to its scaling exponent corresponding to $H = 1/3$. In rain, at "weather scales" (<≈5–10 days), it seems likely that $H > 0$ – as theoretically expected for passive scalars in turbulence – at small scales in space $H \approx 1/3$ (as for the liquid water density, [5]). However at larger scales – at least for the related radar reflectivity and in the horizontal direction – we find that $H = 0.00 \pm 0.01$ [6]. The low H result gives an ex-post-facto justification for the common assumption in the precipitation literature that H is identically zero (e.g. [7–11]).

Unfortunately, as we see in Section 3.1 using the huge CPC hourly precipitation data base, we find in time for rain rates $H \approx 0.17 \pm 0.11$ up to 2–3 days, a result which itself is somewhat dependent on the rain/ no rain threshold of the gauges. This new value is somewhat larger than several older published results on rain; both [12,13] estimate $H \approx -0.1$ in time [14] find $H \approx -0.02$, [15] find $H \approx 0.04$, and [16] finds $H = 0.00 \pm 0.003$. Recently there has been some interesting work on this [17,18] where important differences were found when comparing exponents for the rain rate on all the data (including the zeroes) and those only for the raining part (the support). Using radar data on regions without rain free "holes" it was found that $H \approx 0$ for data with holes, but $H \approx 0.4$ for purely raining regions. These authors also performed numerical simulations that confirmed the strong impact of zeroes on the parameter estimates including the intermittency parameter C_1 discussed below. In a similar vein, we find here on the CPC data that as the threshold increases, H decreases: for example, if thresholds are chosen so that they are exceeded only 3.5% of the time, then from the same data we obtain $H \approx 0.12 \pm 0.11$ while for higher thresholds corresponding to 1% raining, we find $H \approx 0.05 \pm 0.10$ so that these extremes could apparently be generated by a conserved ($H = 0$) process. It is thus significant that the result $H \approx 0.0$ for the spatial reflectivities is valid for a satellite radar whose minimum detectable signal is double the mean and that gives a signal above the noise level only 3.5% of the time. Finally, we should note that various common data analysis techniques exist which are only justified if $H = 0$ so that the common habit of blindly assuming $H = 0$ may have contributed to the current lack of consensus on the scaling properties of rain.

But no matter how rain is related to a multiplicative cascade – no matter what the value of H – there remains the issue of what is the relevant type of cascade. One aspect of this is the now old debate about multifractal universality ([19–21]) which continues today in the guise of (weak) log–Poisson universality, ([22–24]) versus (strong) log–Levy universality ([25,26,13,27,6,28,15,17,18,16,29]). Similarly, the low and zero rain rates are notoriously difficult to accurately measure, and they are prone to spurious breaks and spurious behaviours [30]. This has lead to two alternative modelling approaches. The first assumes that the "support" of the precipitation – where the rate $R > 0$ – is a fractal set [31–33,28,24], the second that the zero rain rate values are the consequence of a combined physical and instrumental thresholding mechanism wherein the rainrate below some low value is set to zero ([5,6,17,18], and see Gires et al. this volume). The former hypothesis is somewhat unsatisfactory – if only because it implies that in the small scale limit, that the rain areas are strictly zero so that finite raining areas depend sensitively on the inner and outer cascade scales. In comparison, the thresholding mechanism implies – as found empirically – that the regions with low (and zero) rates will have poor/broken scaling.

At the other end of the spectrum, the nature of the extreme large rain rates also continues to be debated. Does the rainfall cascade intrinsically generate singularities of all orders (such as the universal multifractal cascades based on Levy generators), or is there an intrinsic physical upper bound (as in the log–Poisson models)? The former generally leads to power law tails on probabilities of extreme rainrates with the maximum on any given realisation being a widely varying random variable. In contrast, the latter implies that rainrates exceeding a critical level are impossible so that the maxima (of series, of radar scans) are roughly constant. Note that these cascades whether with bounded orders of singularities or not, are genuinely intermittent multifractals, they should not be confused with the "Bounded Cascades" introduced by Cahalan and coworkers [34,35] and Menabde et al. [36] in which the cascade is progressively weakened at each step and which ultimately yields processes which in the small scale limit are essentially classical nonintermittent quasi-gaussian process [37].

Even seemingly technical issues can have consequences for the way we analyse the data. For example if we assume that the cascade's scale by scale conservation of turbulent fluxes is rigorously enforced at each cascade step – i.e. that it respects this strong "microcanonical" constraint – then the statistics could be

completely deduced from "weights" or "multipliers" which are simply the empirical ratios of cascade processes at neighbouring resolutions (e.g. differing by a factor of two or four; e.g. [38,8,10,11,24]). However, if the conservation is only on the ensemble – i.e. if it only respects the much weaker "canonical" constraint (corresponding to the more general situation) – then the standard moment-based analysis methods (which involve wide ranges of scales) must be used (see.[39] for a discussion). Finally, the microcanonical assumption also implies a bound on the largest singularity so that it too has implications for the nature of the extremes: unbounded, canonical cascades are necessary to explain power law extreme tails on the probability distributions and numerous such claims have been made, see Section 3.2 for new evidence and a discussion.

While these issues may seem removed from practical applications, this is not the case: their clarification is necessary if only to *measure* space–time rainfall! Indeed, a main conclusion of this paper is that the reconciliation of the scale by scale gauge, remote and reanalysis field statistics will require not only explicit scaling assumptions but also explicit numerical cascade models. These theoretical issues also inform some of the more recent applications of cascades to rain such as to downscaling/disaggregation where current techniques assume rain is a pure multiplicative cascade ($H = 0$) and most of them, that the support is fractal (e.g. [8,10,11,24]).

1.2. Precipitation at global scales

In spite of the now significant literature on cascades and multifractals in precipitation, applications to date have been restricted to regional spatial scales, typically not exceeding the area of a single ground based radar (with linear extents <≈500–1000 km). The only exceptions appear to be the recent global scale study of TRMM satellite radar data [6] which found that the scaling is quite remarkable and extends from kilometres to the size of the earth and [40] that used daily rain rates from gauges with global coverage and attempted to take into account the fractal clustering of stations. The only markedly poor scaling was for the low (and zero) rain rates, and the highest rates at the smallest scales. Yet the former behaved nearly as expected of a scaling process whose reflectivities were effectively "thresholded" by the inadequate dynamical range of the TRMM radar (in this case, the weakest signal it could detect above the noise was double the mean value) while the high rain rate deviations could likely be explained as radar attenuation effects. In other words there was no compelling evidence for a breakdown in the underlying scaling symmetry.

Encouraged by the success of this global analysis, and by the recent finding that the traditionally meteorological state variables (notably the wind, temperature, humidity, geopotential heights) have accurate global scale cascade structures in weather forecast models and reanalyses [41–43] in situ data sets including aircraft [44], and in radiances from satellites.[45], it is natural to compare the planetary scale space–time cascade structure of precipitation from reanalyses, from in situ networks and from satellite radar. In addition, if the spatial scaling continues to essentially planetary scales, then it is natural to interpret the critical scale $\tau_w \approx 5$–10 days as the rough lifetime of planetary scale structures, it defines the upper limit of the weather regime. For $\tau > \tau_w$, the spectrum is relatively flat and it has been proposed that for scales $\tau > \approx 1$ month that it is in fact a Gaussian white noise (e.g. [46]). If true, this would have important implications for both the interpretation and modelling of precipitation. In order to study this, below we exploit both the 29 year gridded hourly CPC data over the US as well as the unique 138 year, 6 hourly global Twentieth Century reanalysis data [47]. Aside from its unique length, the 20CR reanalysis is particular in that it only uses surface pressure and monthly sea surface temperature data as inputs, this leads to very homogeneous data quality over its entire duration.

The basic aim of this paper is thus to use some of the more exceptional global scale precipitation data sets – they collectively span 1 h to 138 years in time and 4.3 to 20,000 km in space – in order to obtain an overall empirical scaling characterisation the space – time scaling of precipitation. Along the way our analyses clarify the fundamental issues raised in the above discussion.

This paper is structured as follows. In Section 2 we review the basic cascade theory needed to understand the analyses and we present the data sets and the basic spatial analyses. In Section 3 we continue to the more involved temporal analyses, presenting in separate sections an analysis of the high and low frequency weather regimes as well as an analysis of the extremes and the temporal cascade structure. In Section 4 we present a discussion of the latitudinal dependence of the precipitation cascade including space–time relations. In Section 5 we conclude.

2. The cascade properties of ground and space radar, gauge networks and reanalysis rain fields

2.1. The basic prediction of multiplicative cascade models

Multiplicative cascade models involve the multiplicative modulation of small structures by larger ones with a basic scale invariant mechanism repeating scale after scale from large to small scales. After a total range of scales λ', the qth order statistical moment of the dimensionless cascade flux φ' is given by the following basic equation:

$$\langle \varphi'^q_{\lambda'} \rangle = \lambda'^{K(q)} \tag{1}$$

$\lambda' = L_{eff}/L_{res}$ is the ratio of the "effective outer scale" L_{eff} to the smallest (resolution) scale of the cascade L_{res}. "$\langle . \rangle$" indicates statistical (ensemble) averaging.

In empirical analyses such as those discussed here, the outer scale is not known *a priori* but is itself a significant empirically determined quantity. We will instead use the symbol λ as the ratio of a convenient reference scale to the smallest resolution and φ will be the usual dimensional flux:

$$M_q = \langle \varphi'^q_{\lambda} \rangle; \quad \varphi' = \frac{\varphi_\lambda}{\langle \varphi \rangle} \tag{2}$$

($\langle \varphi \rangle$ is the ensemble mean large scale flux, i.e. the climatological value, it is independent of scale, hence there is no need for a subscript). Following Eq. (1), the nondimensional qth moment M_q obeys the multiscaling relation:

$$M_q = \lambda'^{K(q)} = \left(\frac{\lambda}{\lambda_{eff}}\right)^{K(q)}; \quad \lambda' = \lambda/\lambda_{eff}; \quad \lambda = L_{earth}/L;$$
$$\lambda_{eff} = L_{earth}/L_{eff} \tag{3}$$

Here, λ is a convenient scale ratio for the spatial analyses, we base it on the largest great circle distance on the earth: $L_{earth} = 20{,}000$ km and the scale ratio $\lambda' = \lambda/\lambda_{eff}$ is the overall ratio from the scale where the cascade started to the resolution scale L, it is determined empirically. From the foregoing discussion we expect $L_{eff} \approx L_{earth}$ so that $\lambda_{eff} \approx 1$ which corresponds to planetary scale cascades. Since even at planetary scales each field nonlinearly interacts with the other fields, it is possible (and we often find) that L_{eff} is somewhat larger than L_{earth}. For the temporal analyses, we simply take the large reference time scale as the total duration of the data set.

In order to investigate possible zonal/meridonal and space/time anisotropies and to test the general predictions of multiplicative cascades (Eq. (1)), we must analyse the data without relying on any specific theories of turbulence; we must use an approach that does not require *a priori* assumptions about the physical nature of

the relevant fluxes; nor of their scale symmetries (isotropic or otherwise). If atmospheric dynamics are controlled by scale invariant turbulent cascades of various (scale by scale) conserved fluxes φ then in a scaling regime, the fluctuations $\Delta R(\Delta x)$ in the rain rate R (or other observable such as wind, temperature or radiance) over a distance Δx are related to the turbulent fluxes by a relation of the form:

$$\Delta R(\Delta x) \approx \varphi \Delta x^H \quad (4)$$

(this is a generalisation of the Kolmogorov law for velocity fluctuations, the latter has $H = 1/3$ and $\varphi = \varepsilon^\eta$, $\eta = 1/3$ where ε is the energy flux to smaller scales). Without knowing η nor H – nor even the physical nature of the flux – we can use this to estimate the normalised flux φ' at the smallest resolution ($\Delta x = l$) of our data:

$$\varphi' = \varphi/\langle\varphi\rangle = \Delta R/\langle\Delta R\rangle \quad (5)$$

Note that if the fluxes are realisations of pure multiplicative cascades then the normalised η powers $\varphi^\eta/\langle\varphi\rangle^\eta$ are also pure multiplicative cascades, so that $\varphi' = \varphi/\langle\varphi\rangle$ is a normalised cascade. The fluctuation, ΔR can be estimated in various ways; in the following (with the exception of Fig. 1b), rather than using fluctuations in space (Δx), we estimate them in time (Δt) we used the 2^{nd} centred differences: $\Delta R(x,y,t) = |R(x,y,t) - (R(x,y,t+\Delta t) + R(x,y,t-\Delta t))/2|$ where Δt is the time difference between successive (x,y) sections. In general, fluctuations are defined using wavelets; the second difference is an extension of the poor man's wavelet (which is the first difference: $\Delta R = R(t+\Delta t) - R(t)$). The second differences are generally adequate when $0 < H < 2$ – and hence for most of our present purposes (see however Section 3.4 where we discuss fluctuations defined by Haar wavelets). The resulting high resolution flux estimates can then be degraded (by averaging) over 1-D "pencils" in (x,y,t) space, i.e. in the east–west, north–south or temporal directions to resolution λ times lower.

2.2. The data sets analysed

2.2.1. The TRMM satellite radar data

One of the data sets we analysed was 5300 orbits of the Tropical Rainfall Measuring Mission (TRMM; the entire year 1998) The reflectivities (Z) were given an attenuation correction and converted into rainrate estimates (R) using the power law $Z = aR^b$ with the recommended TRMM value $b = 1.4$ [48]. In order to check the basic scaling of this surrogate rain rate field (which is "along track", i.e. primarily in the NE or SW directions and nearly instantaneous in time), we estimated the flux from the absolute finite difference (spatial) Laplacian ($\varphi = |R(x,y) - (R(x+l,y) + R(x-l,y) + R(x,y+l) + R(x,y-l))/4|$) where $l = 4.3$ km, the interpixel distance (this is the nominal resolution, but due to the narrow swath, it varied by only about 20%). The results are shown in Fig. 1b which show that with the main exception of the low moments – affected by the low and zero rain rate problems – the scaling is generally well respected over the entire range. There are also deviations for the higher moments at smaller scales these are likely to be consequences of imperfect attenuation corrections; see [6]. Actually, our results are not changed much if we perform the same analysis by directly degrading R (i.e. by taking $\varphi = R$). This is because using the reflectivity directly one obtains $H \approx 0.0 \pm 0.01$ (note that the scaling at the small scales was a little better for Z than for R [6]). Note that here, as for the other moment analyses presented below, the log–log linear regression were forced to go through a common point, the effective external scale of the cascade. The slopes of the lines yield $K(q)$ and numerical derivative of the latter at $q = 1$ gives an estimate of the parameter $K'(q) = C_1$.

In order to compare the TRMM results with those from the gauge network and the reanalyses, we degraded it over 100×100 km boxes between ±40°; the limits were imposed by the orbital parameters. All the data within a four day period (roughly the mean time for the satellite to return to a given location) were averaged to produce a 4 day resolution precipitation map, see Fig. 1a which shows the coverage of a typical example (see Table 1 for a summary of the characteristics of this and the following precipitation products). For this 100×100 km product, the flux was estimated by the centred differences in time ($\varphi = |R(x,y,t) - (R(x,y,t+\Delta t) + R(x,y,t-\Delta t))/2|$). This definition of the flux using the second temporal differences was also used in CPC and ECMWF products discussed below; not much difference was found when the corresponding spatial flux estimate (the absolute Laplacian) was used instead. When averaging (degrading the resolution) of the fluxes along successively the x, y, t directions, we only used "pencils" that had less than 20% missing data.

The moment analyses are shown in Fig. 2 (east–west) and Fig. 3 (north–south); these are not too different from the typically NE or SW along-orbit results (Fig. 1b) except that a strong north–south/east-east anisotropy is evident (at least for the outer scales; see Table 2 and discussion below).

2.2.2. Gridded gauges over the continental US, the CPC network

Since the Z–R transformation has only been theoretically justified using various problematic assumptions (such as the spatial uniformity of the drop size distribution), it is important to compare this satellite rain with in situ (gauge) measurements and to reanalyses. For this purpose, we used NOAA's CPC (Climate Prediction Center), US hourly gridded precipitation (rainrate) product. This product is unique in its high temporal resolution over a large number of contiguous grid points. We selected a (near complete) subset of the CPC data for the 29 years 1948–1976 (at this date there is a data gap of several weeks so that we did not extend the analysis to more recent times). The CPC data was gridded on $2.5° \times 2.0°$ boxes by using a modified Cressman Scheme (an interpolation technique); we used its central rectangular 13×21 point region from: $-122.5°$ to $-72.5°$ longitude (every $2.5° \approx 210$ km at these latitudes), and from 30° to 54° latitude (every 2°, ≈220 km). Each grid box had a near complete ≈257,000 point long hourly series. The spectrum (Fig. 4a) shows very strong annual and diurnal (and subharmonic) spikes so that the data were detrended both annually and daily before determining the fluxes. This detrending somewhat improves the low q scaling without affecting the high q statistics much. The annual detrending was performed by replacing the Fourier components corresponding to frequencies $\omega = \pm(1\ yr)^{-1}$ by the average of the "background" at the neighbouring frequencies. The daily detrending was performed by removing the daily cycle (the latter simultaneously removes or weakens the many subharmonics of the daily cycle). The analysis results are shown in Figs. 2 and 3 showing that the gridded data also have a cascade structure in the east–west and north–south directions, and that the extrapolated outer scale is nearly the same as for the ground and satellite based radar reflectivities in Figs. 2 and 3 (see Table 2).

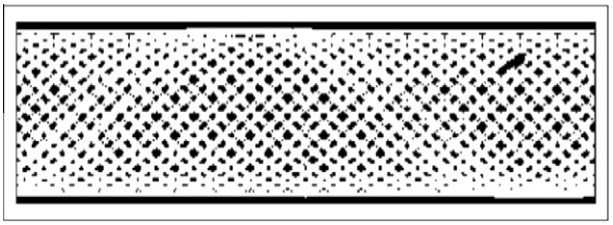

Fig. 1a. This shows a typical 4 day (64 orbit) coverage by the TRMM PR instrument at 100 km resolution. The black indicates the 100×100 km boxes without data; the white those with at least one satellite pass (giving at least 60% coverage of the pixel: the raw data was at 4.3 km resolution and the swath was 220 km wide).

Table 1
The characteristics of the various precipitation data sets discussed in the text. The raw 20 CR data were at 3 h but with the exception of the spectrum (Fig. 4a), we used the data at 6 h resolution.

	Spatial resolution (EWxNS)	Spatial extent EW	Spatial extent NS	Temporal resolution	Length of record
ECMWF (interim reanalysis)	1.5° × 1.5°	360°	180°	3 h	3 months (1/06–3/06)
CPC (Climate Prediction Center, gages)	2.5° × 2°	122.5° − 72.5°W (≈4000 km)	30° − 54°(≈3000 km)	1 h	29 years (1947–1976)
TRMM (satellite radar)	100 × 100 km	360°	40S°–40 N°	4 days	1 year, 1998 (5300 orbits)
20CR	2° × 2°	360°	2° (only 44°–46° analysed)	6 hrs	138 years (1871–2008)

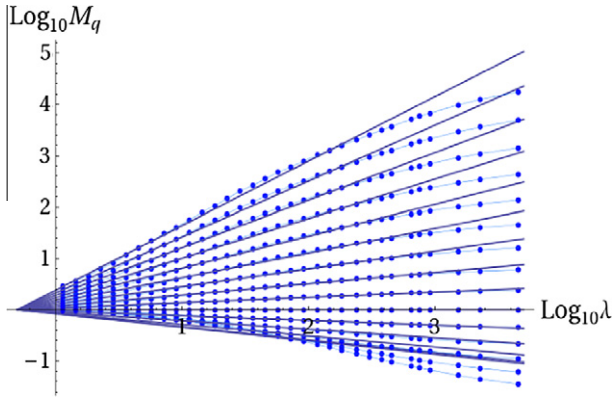

Fig. 1b. The nondimensional moments M_q from the TRMM rainrate estimates. The moments are for $q = 0$, 0.2, 0.4, ...3, outer scale ≈39,000 km, $C_1 = 0.48$, for the rainrates estimated from the reflectivity with $b = 1.4$ along the orbit direction, spatial resolution 4.3 km. $\lambda = 1$ corresponds to 20,000 km. The poor scaling (curvature) for the low q values are likely to be artefacts of the fairly high minimum detectable signal, at the high q values by attentuation. $L_{ref} = 20{,}000$ km so that $\lambda = 1$ corresponds to 20,000 km. The regression lines were for scales >20 km.

2.2.3. The ECMWF and Twentieth Century reanalyses

Before making a quantitative satellite/gauge intercomparison, let us first consider the corresponding analyses on the ECMWF interim "stratiform rain" product (at the time of the research the new "convective precipitation" product was not yet available). We used the first 3 months of 2006 at the full (3 h) resolution. The results in the east–west and north–south directions are also shown in Figs. 2 and 3, the parameters and those of the other products are shown in Table 2. We have also made more limited use of the uniquely long (1871–2008) Twentieth Century (20CR) reanalysis which especially helps to clarify the low frequency behaviour (Section 3.4). As a first comment, from the figure we see that the basic cascade structures are quite well respected and are very similar for each of the data sets. Indeed, for a given data set, when averaged of all scales and moments $q \leqslant 2$, the deviations from log–log linearity are of the order of a few percent. This is significantly smaller than the variations between the different data sets which in some cases are as large as a factor of 2 (e.g. the $q = 2$ moments at 400 km for the 20CR and TRMM data). Since all the rain measurement techniques have various problems, it would not be surprising if the differences reflect the limitations of the measurement techniques rather than a breakdown in the scaling symmetries. Indeed, in order to improve the measurement techniques it is tempting to extrapolate the observed scaling to subsensor scales and use this heterogeneity assumption to replace the homogeneity assumptions which are typically made in when interpreting gage networks, radar or reanalysis fields.

2.2.4. Scale by scale intercomparison: the spatial scaling

For a given moment order q, we find that the exponents $K(q)$ are much higher than when compared with any of the usual meteorological fields (e.g. for temperature, wind, humidity). A simple way to quantify this is to use the parameter $C_1 = K'(1)$ which characterises the intermittency near the mean: theoretically, C_1 is the codimension of the fractal set which gives the dominant contribution to the mean. From Table 2 we see that the values for C_1 for precipitation which are in the range 0.25 to 0.5; this may be compared to the values for the state variables which are much smaller: typically in the range 0.05–0.10 see [42,49] (although the C_1 for the turbulent energy flux is also ≈0.5, it is not observed directly in the same way as precipitation). This confirms our intuition about rain: that it is much more intermittent than the other atmospheric fields (recall that C_1 is an exponent so that for statistics near the mean ($q = 1$)), the difference between a field with $C_1 = 0.05$ and one with 0.5 is a factor $\lambda^{0.05}$ compared to $\lambda^{0.5}$ which – depending on the range of scales λ – can be enormous. We also note the reasonable agreement between the outer scale estimates: $(39 \pm 10) \times 10^3$ km in the east- west direction and $(27 \pm 9) \times 10^3$ km in the north/south direction (the spread is the variation from one product to another and the raw outer scale estimates in the table are only quoted to within 1 dBλ i.e. to the nearest tenth of an order of magnitude, to within a factor ≈1.25). Taking the ratio of the east–west to north–south outer scales gives us the "trivial anisotropy", i.e. the typical aspect ratio in the horizontal (assuming that there is no differential, scale by scale anisotropy). The ratios of the means (excluding the 20CR data which were analysed only zonally) gives a factor 1.61 which is almost the same as for the mean of the state variables (wind, temperature and geopotential height estimated from the other ECMWF interim fields, see [43]).

Table 2
An comparison of some of the cascade parameters for the precipitation products discussed in the text. The temporal analyses are discussed in Sections 3.1 and 3.4. The zonal/meridional aspect ratios a are: 1.6, 1.3, 2.5, for the ECMWF, CPC, TRMM fields respectively. The 20CR data set was mostly used because of its long length, the analyses were only at 45°N.

	ECMWF		CPC		TRMM $R \propto Z^{1/1.4}$		20CR	
	C_1	L_{eff} or τ_{eff}	C_1	L_{eff} or τ_{eff}	C_1	L_{eff} or τ_{eff}	C_1	L_{eff} or τ_{eff}
East West	0.39	50,000 km	0.27	40,000 km	0.49	40,000 km	0.26	25,000 km
North South	0.45	32,000 km	0.32	16,000 km	0.51	32,000 km	–	–
Time	0.34	71 days	0.30	1100 days	0.37	42 days	0.22	50 days

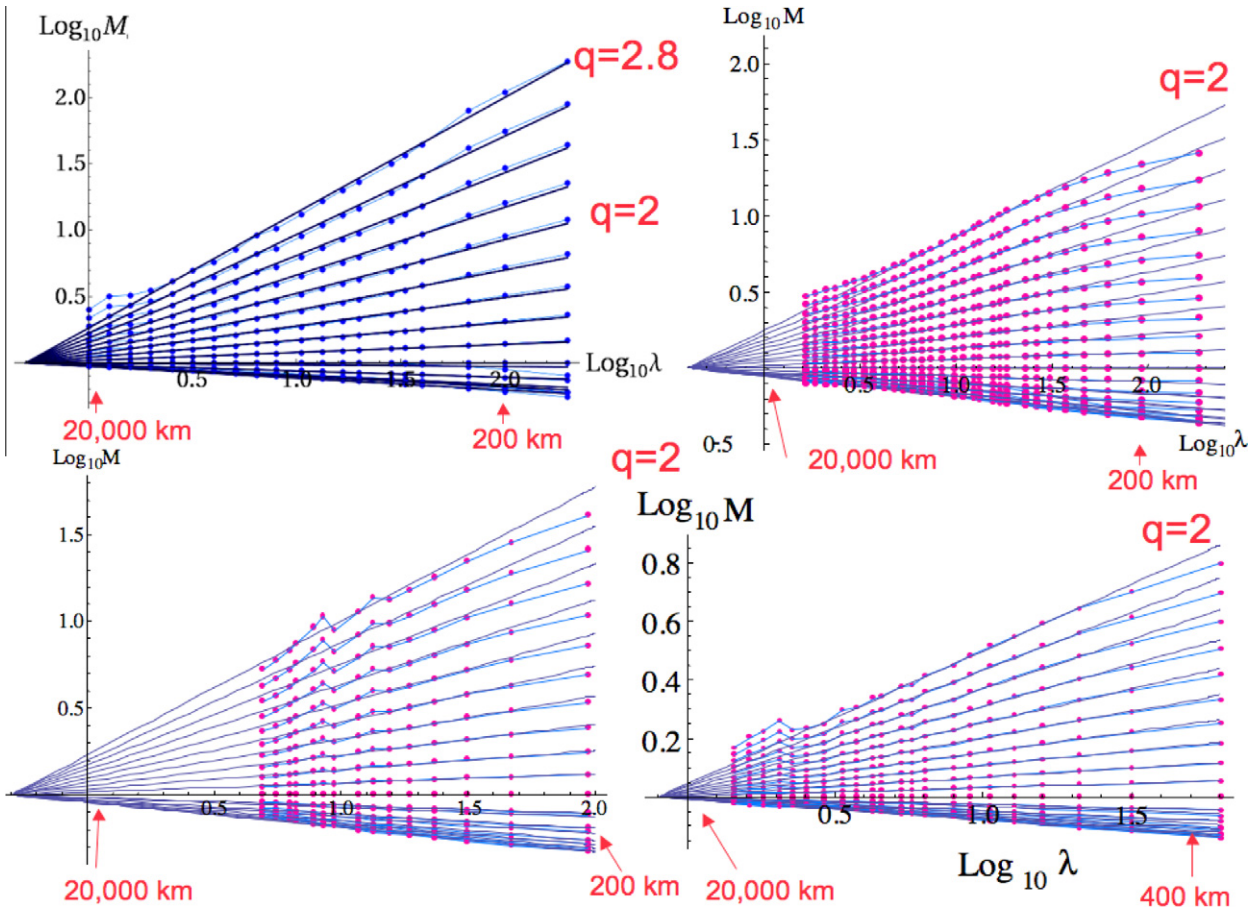

Fig. 2. East–west analyses of the gridded precipitation products discussed in the text. Note that the vertical scales are different. The regressions were over the scales 400–5000 km.

The precise variations of the C_1 values in Table 2 are not so easy to explain. First, the east–west C_1 values are not quite the same as those in the north–south direction. Depending on the product, the differences are between 4 and 16% in the exponents, if these variations are statistically significant they would indicate systematic scale by scale scaling anisotropies. However, it is not obvious that they are in fact significant. On the one hand, even with all this data, statistical exponents are very hard to accurately estimate; this is especially true since the large C_1 values indicate huge sample to sample variability (intermittency). On the other hand, there are fairly large variations from one product to another – larger than the north–south/east–west differences – and in any case, the east–west values are not even systematically larger than the north–south ones (they are smaller in the ECMWF product, larger in the others). For the moment we we may reasonably consider that the C_1's are the same in the east–west and north south directions so that the trivial anisotropy is real, whereas the scale by scale anisotropy (reflected in directional variations in C_1) may be an artefact.

There remains the interesting task of understanding the product-to-product differences and this should shed light not only on the fundamental nature of rain, but also on the optimum way of estimating rainrates from in situ and remote measurements and of simulating rain in numerical models. Recall that since we are discussing exponents that characterise the scale by scale statistical properties, for the products to agree about the rain rate at any particular space–time point, it is necessary – but not sufficient – that they have identical cascade parameters (both exponents and outer scales). Although at this point it would be quite possible – following the detailed TRMM analysis in [6] – to quantify scale by scale, moment by moment, product by product the deviations from perfect log–log linear scaling, along with detailed parameter uncertainty estimates, at present this does not seem worthwhile. The reason is that the product to product variability – which presumably reflects instrumental limitations – appears to be larger than the deviations of any given product form log–log linearity. It therefore would be more reasonable to expend effort on modelling and understanding the instrumental problems rather than attempting overly precise characterisations of uncertainties and biases which may well be partially if not largely instrumentally generated.

A full characterisation of the cascade requires the full $K(q)$ function; in practice, this must be parametrized. If the precipitation process is the domain of attraction of universal multifractals, then $K(q) = C_1(q^\alpha - q)/(\alpha - 1)$ where $0 \leqslant \alpha \leqslant 2$ is the Levy index. However, in Table 2 we did not include estimates of the Levy index α (which can be estimated as $K''(1)/K'(1)$, i.e. it characterises the curvature near the mean $q = 1$): its estimation depends sensitively on the low values of the rainrate and these are poorly measured. Reference [6] pays much attention to this and with the help of cascade models concludes that $\alpha \approx 1.5$ but the evidence is still not compelling (see e.g. [50] for a review of empirical estimates). We defer the discussion of α to a future paper.

The spatial values of C_1 in Table 2 can be compared with those in the literature, notably [40], $C_1 \approx 0.16$; [25], $C_1 \approx 0.02$–0.1 [51], $C_1 \approx 0.35 \pm 0.2$ [17,18], $C_1 \approx 0.5$, $H \approx 0$ for data with zeroes, $C_1 \approx 0.15$, $H \approx 0.4$ for data without zeroes. These estimates are (mostly) from gauges (although the latter reference also consider radar scans); we see that our values are more in accord with the more recent estimates but there is still much uncertainty. Understanding the sensitivity to zeroes thus seems to hold the key to a

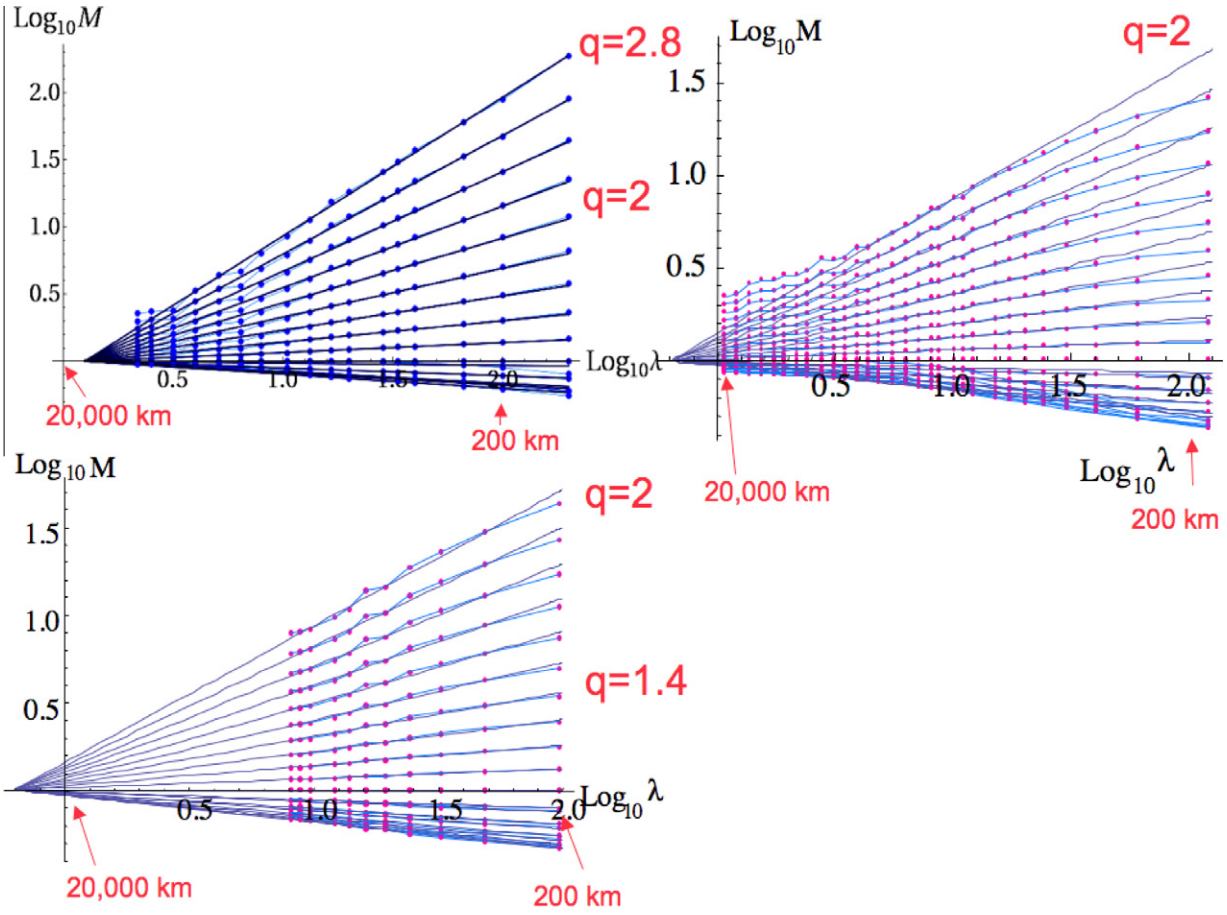

Fig. 3. Same as Fig. 2 but for the north–south analyses. The 20CR data was at 45°N and this was not analysed in the meridional direction. The regressions were over the scales 400–5000 km.

better understanding of the variation in the literature of both H and C_1 parameters.

Upper left: The TRMM 100x100, 4 day averaged product.
Upper right: The ECMWF interim stratiform rain product (all latitudes were used). Note that the data were degraded in constant angle bins so that the outer scale is 180°. To compare with the other analyses, a mean map factor of 0.69 has been applied (the mean east–west outer scale was ≈14,000 km).
Lower left: The CPC hourly gridded rainfall product (US only).
Lower right: The 20CR reanalysis at 45°N only (data at 4° resolution).
Upper left: The TRMM 100 × 100, 4 day averaged product.
Upper right: The ECMWF interim stratiform rain product.
Lower left: The CPC hourly gridded rainfall product (US only).

3. Temporal analyses

3.1. The weather regime: estimating H

Dimensionally, space and time are connected by a velocity; physically in fluid systems by advection. If the relevant velocity is scaling and – and it is in reanalyses [41,43] and in aircraft data (although see the debate [52]) - then we expect the spatial scaling of precipitation to be accompanied by temporal scaling. Before taking a look at the analyses of the cascade structure (i.e. the fluxes), we can therefore consider the 1-D temporal spectra of the CPC,

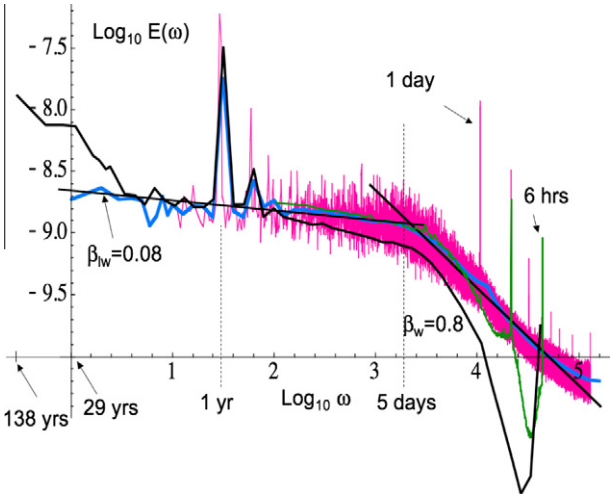

Fig. 4a. A comparison of the temporal spectra of the CPC data (red) and the ECMWF 3 hourly data set (green). The blue curve is the CPC spectrum averaged over logarithmically spaced frequency bins (10 per order of magnitude). The long black curve is from the 20CR at 45°N, from the full 3 h resolution data (from 1871–2008). The transition scale from the high frequency weather regime and low frequency weather-climate regime is indicated by the dashed line at periods of 5 days. The axis is in units such that $\omega = 1$ is $(29\ yrs)^{-1}$; i.e. the full length of the CPC series. There are three reference lines with absolute slopes indicated; the value 0.08 is from the Haar structure function analysis (Section 3.4) from 3 months to 29 years. (For interpretation of the references to colour in this figure legend, the reader is referred to the web version of this article.)

ECMWF and 20CR series (i.e. the average of the temporal spectra from each pixel), Fig. 4a. We did not include the TRMM spectrum since the series had too many missing data points (see Fig. 1a). From Fig. 4a we can see that as for all meteorological fields, there are two regimes: a high frequency (usual) "weather" regime and a "low frequency weather" regime'. As indicated in the figure, the transition is at about 5 days. Starting with the top of the atmosphere solar flux ≈ 1 kW/m^2, this transition time can be theoretically deduced essentially from first principles. By using a conversion efficiency of 2% to kinetic energy we can obtain the mean tropospheric turbulent energy flux $\varepsilon \approx 10^{-3}$ m^2/s^3 so that the lifetime of planetary structures (at scale $L_e \approx 2 \times 10^7$ m) is $\tau_w = \varepsilon^{-1/3} L^{2/3} \approx 10$ days. As argued in [53,42,49], for scales $\tau > \tau_w$, we have "low frequency weather" characterised by a "spectral plateau" with relatively small exponent spectral $\beta = \beta_{lw}$ defined by the power spectrum $E(\omega) \approx \omega^{-\beta}$, where ω is the frequency. We return to this regime in Section 3.4.

From Fig. 4a we see that the CPC, ECMWF and 20CR spectra agree quite well for durations longer than one day; for higher frequencies, the 20CR and especially the ECMWF spectra are too smooth; they have small diurnal peaks but respectively large 12 and 6 h peaks. The more trustworthy CPC spectra indicate that at high frequencies $\beta_w \approx 0.8$. More refined analyses obtained from each CPC grid point series and estimating β_w using frequencies $>(2\ days)^{-1}$ yields $\beta_w = 0.76 \pm 0.23$ where the spread is from series to series (i.e. grid point to grid point). Since the spectrum is a second order ($q = 2$) moment, from Eq. (4) we find that $\beta = 1 + 2H - K(2)$ and from the (cascade) analysis of the moments in time (Fig. 5) we find the temporal CPC $q = 2$ exponent $K(2) = 0.59$, yielding the estimate $H \approx 0.17 \pm 0.11$. We therefore see that at least for the CPC data that it is important to perform the cascade (moment) analyses on the fluxes (estimated here by the absolute second time differences) rather than directly on the rainrates.

3.2. The extreme rain rates; estimating q_D

We mentioned that a feature of (general) canonical cascades with unbounded orders of singularities is that they display non-classical probability distributions with power law tails. This implies that extreme values occur much more frequently than predicted by classical "thin" (exponential) tailed distributions or even than predicted by intermediate "long" log-normal type tails. Such power law distributions are of the form:

$$\Pr(\Delta R > s) \approx s^{-q_D}; \quad s \gg 1 \tag{6}$$

where $\Pr(\Delta R > s)$ is the probability of a rainrate fluctuation ΔR exceeding a fixed threshold s, "Pr" indicates "probability" (strictly speaking, this is one minus the Cumulative Distribution Function i.e. 1-CDF). q_D is the critical exponent; the subscript "D" indicates that we expect the value of q_D to depend not only on the "bare" cascade statistics (i.e. on $K(q)$) but also on the dimension of space–time D over which the rain rate is "dressed" (averaged); this is true as long as the averaging scale is much larger than the inner cascade scale which is sub-metric. All the statistical moments $\langle \Delta R^q \rangle \to \infty$ for $q \geqslant q_D$ (hence we limited our study to $q \leqslant 3$ to avoid possible divergences).

There is increasing evidence that precipitation probability distributions have power law tails. For example [19], claimed a probability exponent $q_D \approx 1.1$ for radar reflectivities, and for raindrop volumes [5] found $q_D \approx 5$. For the rain rate there is even an emerging consensus on the value $q_D \approx 3$; for example at various resolutions, [54] claimed $q_D \approx 3.5$; [62] claimed $q_D \approx 2.8$–8.5 [12], $q_D \approx 3.6 \pm 0.07$ [55], $q_D \approx 2$ [13], $q_D \approx 3.5$ [56], $q_D \approx 4.0$ [57], $q_D \approx 3$ [58], $q_D \approx 2.9 \pm 0.7$. Finally, on the basis of a compound Poisson-cascade process reference [59] theoretically predicted that for

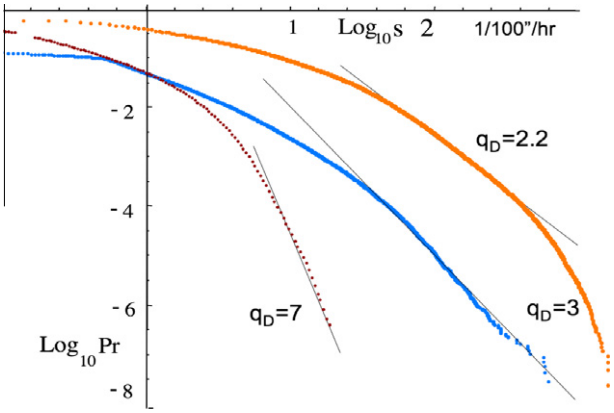

Fig. 4b. This figure shows the $\log_{10}$ of the probability distribution $Pr(\Delta R > s)$ of the absolute rain rate difference ΔR for the CPC hourly gauges (middle, blue) and the daily ECMWF reanalysis (orange, top, for 2005–2008, multiplied by a factor 4 for clarity) and the 138 year long 20CR 6 hourly data (at 45°N only, shown in red, left), all as functions of the $\log_{10}$ threshold s. For the CPC data there were $13 \times 21 = 273$ CPC series, each 257,000 h long ($\approx 7.0 \times 10^7$ points total); the ECMWF had 1460 days with 29040 grid points each (a total of $\approx 4.2 \times 10^7$ points) while the 20CR data was every 2nd longitudinal pixel at 45°N for a total of 1.8×10^7 points. The reference lines have $q_D = 3$ (which is very close to the tail of the CPC data), $q_D = 2.2$ which is plausible for an intermediate region of the ECMWF data and for the 20CR data, $q_D = 7$ which is not so convincing but is nevertheless shown for reference. The units of s are hundredths of inches per hour. The differences in the amplitudes are partially due to the different time lags (Δt).

the total liquid water in a region obeying passive scalar (Corrsin–Obhukhov) statistics, that $q_D = 3$ (exactly) and confirmed the result using stereophotography of rain drops. In Fig. 4b, using the very large (hourly) CPC data base we give more evidence that $q_D \approx 3$ for the rain rate – over a range of factor of 10^3–10^4 in probability. In contrast, the figure shows that the ECMWF and 20CR probability distribution (for daily and six-hourly – not hourly – differences) while being similar in shape for the smaller fluctuations appears to be "truncated" at the largest fluctuations. This suggests that the reanalyses have trouble estimating extreme rain events. Similarly, [6] considered in some detail the extremes of the TRMM reflectivities (Z) and concluded although there was some evidence for $q_{DZ} \approx 2$ for Z (corresponding to $q_{DR} \approx b q_{DZ} \approx 2.8$; with $Z = aR^b$, $b = 1.4$) but that due to the attenuation at large Z, (which was not sufficiently corrected), that the extremes were truncated; hence we did not reconsider the TRMM probabilities here.

The existence of a finite exponent q_D is primae facea evidence that the rain process is capable of occasionally producing singularities of very high orders so that *a priori*, models with unbounded orders of singularity should be used. This rules out microcanonical cascades, Log-Poisson cascades or universal multifractal cascades with Levy index $\alpha < 1$ (although the latter models could conceivably generate finite q_D's if the parameters were carefully chosen).

3.3. The temporal cascade structure

The temporal parameters for the precipitation fields were already shown in Table 2. In spite of the fact that the temporal C_1 estimates are not so different (0.31 ± 0.07), the external scales vary considerably with the TRMM external scale ($\tau_{eff} \approx 3$ years) being about 20 times larger than that of the CPC, ECMWF and 20CR reanalysis products of the estimate $\tau_{eff} \approx 90$ days from [16] using gauges. In any case, although it is much larger than the external scales of other meteorological fields, it is comparable to the outer scale of the ocean variability. Lovejoy and Schertzer [60] show that for the ocean surface $\varepsilon_o \approx 10^{-8}$ m^2/s^3 which implies $\tau_o = \varepsilon^{-1/3} L_e^{2/3} \approx 1$ year. Since the TRMM data are mostly over the

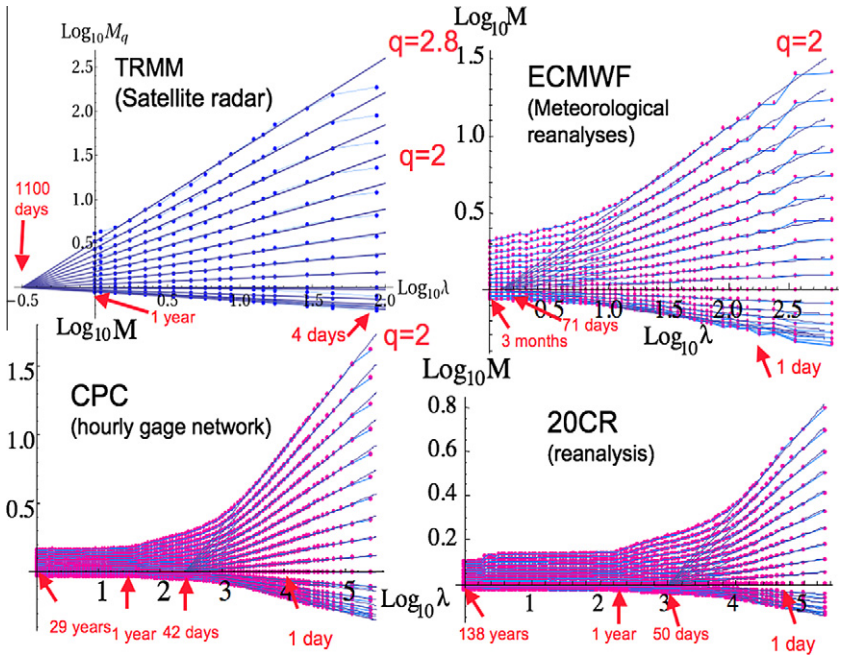

Fig. 5. Temporal analyses of precipitation products. The 2nd time flux for the 100 × 100 km gridded (4 day resolution) TRMM radar satellite rain rate estimates (upper left), for the 3 months of the 3 hourly ECMWF interim stratiform rain product (upper right) and 29 years of NOAA's CPC hourly gridded surface raingauge network (lower left). Note the variation in the vertical scale. These are the temporal analyses corresponding to the spatial analyses presented in Figs. 2, 3. We have added (lower right) the unique very long Twentieth Century reanalysis product analysed at 45°N at 2° resolution in space and 6 h in time from 1871–2008. Note that there is an indication of a second lower intermittency cascades from about 10 days to 1 year. The regression were performed over the range of scales 8 days to 1 year (TRMM), 6 h to 10 days (ECMWF), 1 h to 10 days (CPC) and 6 h to 4 days (20CR).

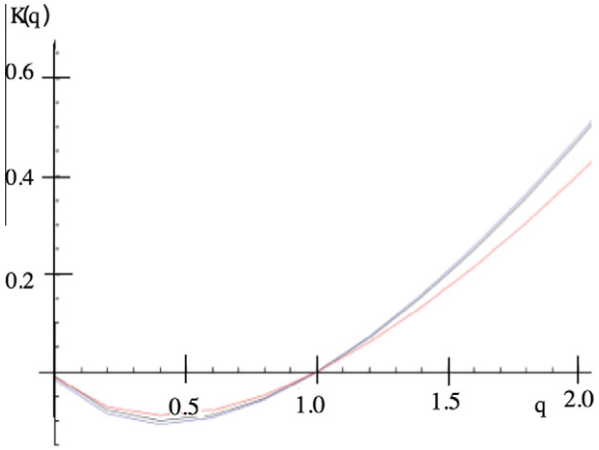

Fig. 6a. The $K(q)$ for the TRMM PR instrument at 100 km, 4 day resolution. On right, the top is the north–south curve, middle is the east–west, the bottom is time.

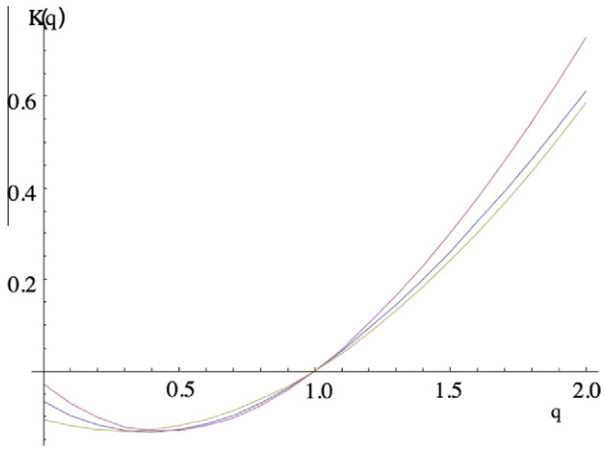

Fig. 6b. ECMWF 3 h, on right, the top is the north–south curve, middle is the east–west, the bottom is time.

ocean this could be an explanation for the large TRMM τ_{eff}. It should be noted that the disagreements in the moments at measured scales are not as large as they might seem at first sight. This is because a large (scale by scale) variability indicated by a large C_1 can be partially offset by a small external scale and from Table 2, we see an inverse correlation between the C_1 values and the external scales: consequently the actual moments in Fig. 5 are fairly similar for the CPC in situ and ECMWF interim products.

Although there are still anomalies, it seems that cascade exponents in horizontal space and in time are compatible with the hypothesis that they have the same values (i.e. it seems likely that the small remaining differences are due to various unresolved data measurement, calibration and interpretation issues). Since the α estimates are not too precise (due to the zero rain rate problem which tends to seriously bias them towards low α values), we can attempt to substantiate this by comparing spatial and temporal C_1 estimates (see Table 2), as well as the $K(q)$ curves (6a–6c). These indicate that the conclusions drawn from the variations in C_1 are relatively robust (see Fig. 6d).

The temporal estimates of C_1 in Table 2 can be compared with those in the literature, notably $C_1 \approx 0.6$ [40]; $C_1 \approx 0.2$ [61]; $C_1 \approx 0.6$ [54]; $C_1 \approx 0.04$–0.19 [62]; $C_1 \approx 0.30$–0.51 [13,14]; $C_1 \approx 0.344$, 0.303 [51,56]; $C_1 \approx 0.38 \pm 0.02$, 0.40 ± 0.1 [51]; $C_1 \approx 0.345 \pm 0.038$ [27]; $C_1 \approx 0.434 \pm 0.005$ [15,27]; $C_1 \approx 0.38$ [16]; $C_1 \approx 0.47 \pm 0.08$ [58]. These are all from gauges; a radar estimate from [40], gives $C_1 \approx 0.6$. We see that – as for the spatial C_1

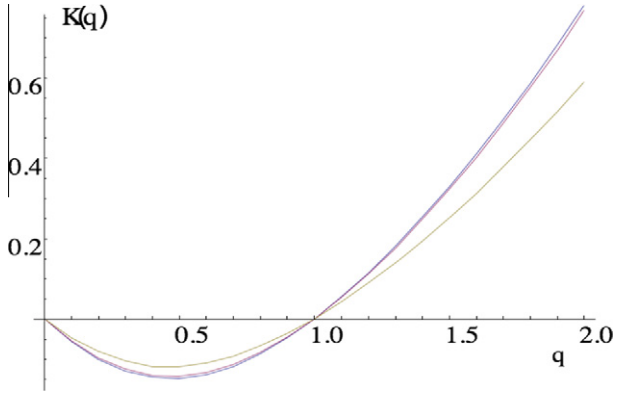

Fig. 6c. CPC: on right, the top is the north–south curve, middle is time, the bottom is east–west.

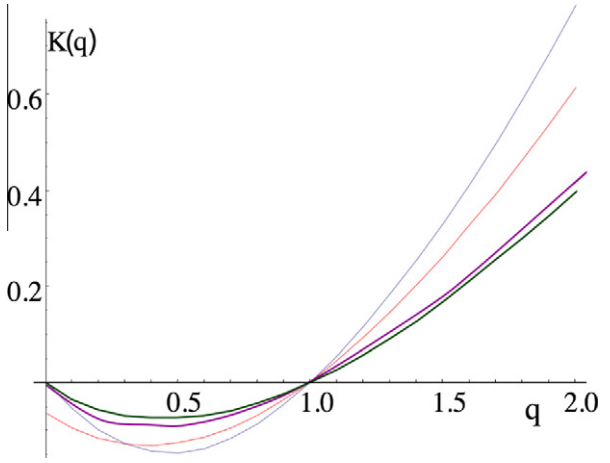

Fig. 6d. This is an intercomparison of the zonal (east–west) $K(q)$ curves from the analyses of Figs. 2, 3, 5 (extracts from Figs. 6a, 6b, 6c, and the 20CR result at 45°N). On the right, top to bottom: we have the CPC (gauges), next from the ECMWF interim (reanalyses), next is from the TRMM (satellite radar) data, and the bottom, is the 20CR result.

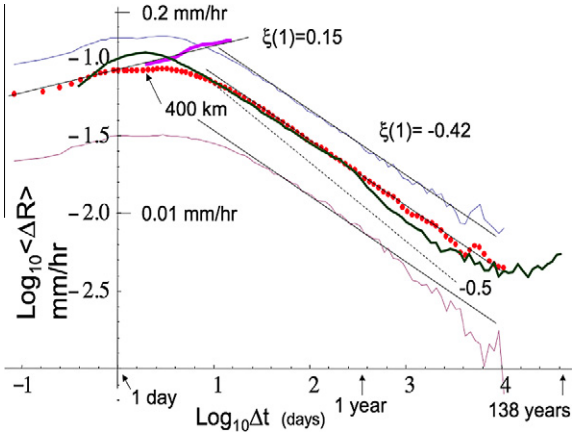

Fig. 7a. A comparison of the first order ($q = 1$) Haar structure function analysis of the CPC (whole grid, resolution, 1 h, 29 years, red (dots) mean, thin lines are the grid point to grid point spread; one standard deviation intervals) and 20CR reanalysis at 45°N (6 hours, 2° resolution, 138 years, thick green line). The short thick purple line (upper right) is the CPC spatial analysis in the east–west direction; the common reference line corresponds to a speed of 280 *km/day*. The reference lines with corresponding slopes are indicated. The magnitudes of the fluctuation rain rates indicate the rough magnitudes, they are accurate to ≈ ± 40%. The line slope − 0.5 is the behaviour expected for Gaussian white noise.

estimates – our values are more in accord with the more recent values but there is still much uncertainty in the estimates, and again the zero/low rain rate issue is a likely source of this uncertainty [5,18].

3.4. The low frequency weather regime: white noise or long range statistical dependencies?

We mentioned in Section 3.1 that the lifetime of planetary scale structures τ_w was about 5–10 days and we discussed the precipitation statistics in the high frequency weather regime ($\tau < \tau_w$). The scale τ_w marks the beginning of a qualitatively new "low frequency weather regime" which extends out to the time scale $\tau_c \gg \tau_w$ after which the spectral exponent β increases again ($\beta_c > \beta_{lw}$); as discussed in [60], this is the climate regime proper. According to paleotemperature data this regime apparently continues to interglacial scales of the order of 50 kyrs (see [49] for a review).

According to the predictions of cascade models, the key difference between the weather and low frequency weather is that at higher "weather" frequencies $\omega > \omega_w$ (where $\omega_w = \tau_w^{-1}$), the fluctuation exponent $H > 0$ so that fluctuations $\Delta R \approx \Delta t^H$ grow with increasing time lag Δt whereas for $\omega < \omega_w$, $H < 0$ so that on the contrary they are reduced in amplitude as the scale Δt is increased. In the low frequency weather regime $\tau > \tau_w$, we find below $K(2) \approx 0.07$ which is not so large so that $\beta \approx 1 + 2H$ and $H > 0$, $H < 0$ corresponds to $\beta > 1$, $\beta < 1$ respectively. For $\omega < \omega_w$; log–log spectra are indeed fairly flat "spectral plateaus"; see Fig. 4a where we see that the low frequency CPC exponent is $\beta_{lw} \approx 0.08$. For $\omega > \omega_w$ the fluctuations depend on interactions in both space and in time, whereas at lower frequencies, only the temporal interactions are important so that τ_w marks a "dimensional transition" [42]. For $\omega < \omega_w$ cascade models predict a low frequency regime with spectral exponents that are insensitive to the high frequency weather statistics. Surprisingly they depend primarily on the overall scale range over which the cascade operates (the ratio ω_w/ω_c), with $0.2 < \beta_{lw} < 0.4$ predicted for $\omega_w/\omega_c \approx 10^3$–$10^5$. Since the ocean has a similar transition but at $\tau_o \approx 1$ year similar coupled ocean–atmosphere models predict $\beta_{lw} \approx 0.6$ for the analogous "low frequency ocean weather" [60].

We have seen that for rain, β_{lw} is close to zero, which is the value that would be obtained for Gaussian white noise. Indeed there have been claims that monthly rainfall is exactly a Gaussian white noise i.e. $K(q) = 0$; e.g. [63,46]. One should be sceptical of these claims on both physical and statistical grounds. First, Gaussian white noise in precipitation would be uncorrelated and this would contradict the meteorological phenomenology of "clustering" of rainy months, years, decades which is observed even after the removal of seasonal effects. Second, $\beta = 0$ does not imply $K(q) = 0$, but only the weaker condition $2H = K(2)$, so that we cannot conclude there is white noise simply on the basis of the value of the spectral exponent.

In order to obtain a more sensitive assessment of the low frequency precipitation regime, rather than use the second order statistic (the spectrum) corrected for intermittency, we can directly consider the statistics of the mean fluctuations of ΔR. The usual way to define fluctuations is simply as a difference: $\Delta R(\Delta t) = R(t + \Delta t) - R(t)$, this is the "poor man's wavelet" (in Section 2.1 we used the 2nd differences). From the fluctuations, the scaling exponents can be estimated from the qth order moments: $\langle \Delta R(\Delta t)^q \rangle \approx \Delta t^{\xi(q)}$ with structure function exponent $\xi(q) = qH - K(q)$. A limitation of these difference (poor man's wavelet) structure functions is that the fluctuation ΔR is only dominated by the scales near Δt (i.e. the frequencies near $1/\Delta t$) if $0 < H < 1$ (i.e. roughly, for $3 > \beta > 1$). This means that if H is outside this range that the structure function will not capture the scaling of ΔR with

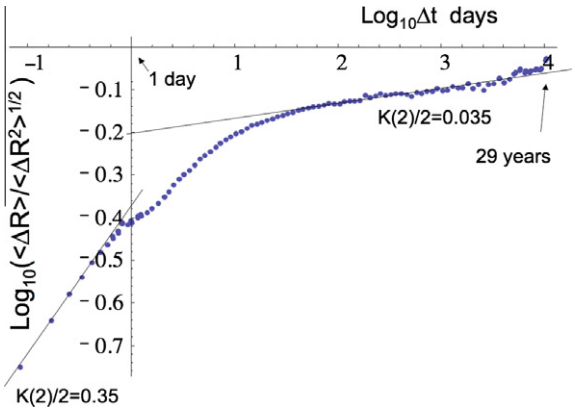

Fig. 7b. This shows the ratio of the mean $q = 1$ and RMS fluctuations for the CPC data set. Reference lines have slopes $K(2)/2 \approx C_1$ and shows the transition from high intermittency behaviour at scales less than a few days (the "weather regime") to low but not insignificant intermittency behaviour at scales of months to years (the "low frequency weather regime"). Gaussian white noise would be flat ($K(2) = 0$).

Table 3
This shows various Haar estimated exponents for the CPC data base. The figures with the one standard deviation spread are the means of the grid point by grid point exponents (with the indicated spread), the figures without spreads are the exponents of the ensemble statistics (i.e. for each parameter the top row is the mean of the exponents, the row below is the exponent of the mean). For Gaussian white noise $\xi(2)/2 = H = 1/2$, $\beta = 0$.

	1 h < Δt < 5 days	2 months < Δt < 3 years	3 months < Δt < 29 years
H	0.092 ± 0.076 0.093	−0.436 ± 0.063 −0.434	−0.43 ± 0.073 −0.419
$\xi(2)/2$	−0.147 ± 0.107 −0.16	−0468 ± 0.056 −0.456	−0.47 ± 0.075 −0.44
β	0.71 ± 0.21 0.68	0.07 ± 0.11 0.09	0.06 ± 0.15 0.08

Δt. Since for scales $\tau > \tau_w$ we have seen that β is close to 0, $H < 0$, we must therefore estimate the fluctuations using other wavelets. The Haar wavelet is convenient and the corresponding Haar fluctuations at scale Δt can easily be computed by introducing the running integral/sum $s(t)$:

$$\Delta R = \frac{2}{\Delta t}\left[\left(s\left(t+\frac{\Delta t}{2}\right)+s\left(t-\frac{\Delta t}{2}\right)\right)-2s(t)\right];$$
$$s(t) = \int_0^t R(t')dt' \quad (7)$$

$\Delta R(\Delta t)$ is proportional to the difference between the means of the first and second halves of the interval. Estimatving structure functions $\langle \Delta R^q \rangle$ with this definition of fluctuation gives correct scaling exponents for $1 < H < -1$ (i.e. ignoring intermittency, for $3 > \beta > -1$) (see [63] for a discussion of applications to multifractals). In Fig. 7a we show $\langle \Delta R \rangle \approx \Delta t^{\xi(1)}$ as estimated by Haar wavelets on both the CPC hourly gridded gauge data and the 20CR reanalysis at 45°N. Due to scale by scale conservation of the cascade, $K(1) = 0$ so that we obtain $\xi(1) = H$. For $\Delta t < \approx 2$ days, we see $H \approx 0.15$ (essentially the same as deduced from the spectrum in Section 3.1). We have also estimated the Haar structure function in space in the zonal direction; we see that it is essentially identical to the time behaviour if a space–time transformation velocity of 280 km/day is used; we discuss this in Section 4.

Turning to the low frequency weather regime, $\tau > \tau_w$, we see that for $\Delta t > \approx 10$ days, $H_{lw} \approx -0.42$ and this is convincingly different from the value −0.5 predicted for Gaussian white noise. In addition, we see that the 20CR and CPC fluctuations are quite sim-

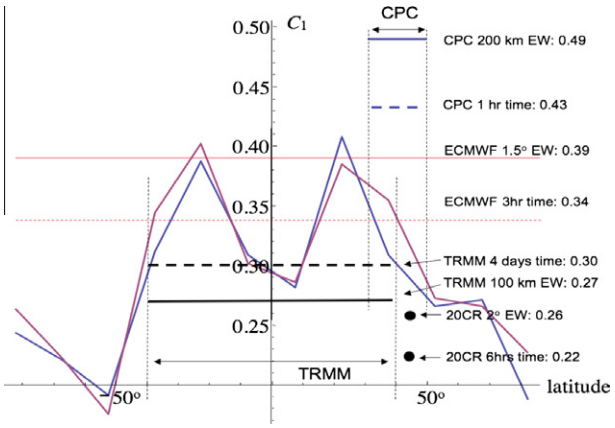

Fig. 8a. This compares the latitude dependence of the zonal and temporal C_1 from daily ECMWF reanalyses (2005–2008) (blue and red curves respectively) with the global mean ECMWF reanalyses (every three hours, red flat lines) and the CPC (blue flat lines, continental US gauges) data (hourly) and the TRMM satellite radar data (4 day resolution); dashed lines are for the temporal analyses, solid for the zonal analyses. For the latter two, the latitude ranges are indicated by dashed lines. (For interpretation of the references to colour in this figure legend, the reader is referred to the web version of this article.)

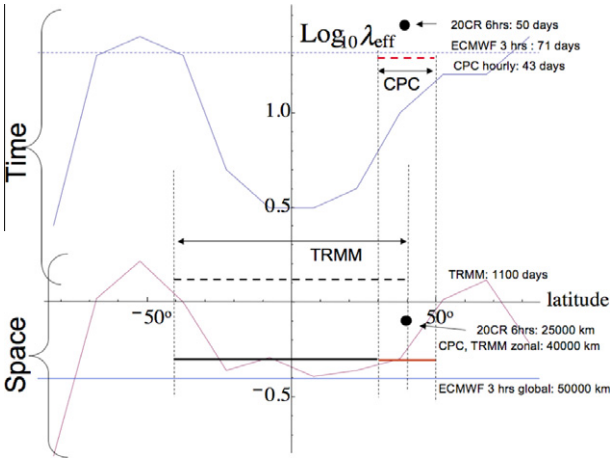

Fig. 8b. This shows the latitude dependence of the zonal spatial outer scale (red) and temporal outer scales (blue) from the daily ECMWF reanalyses from 2005–2008 (same as in Fig. 8a). The reference scales defining λ_{eff} are 20000 *km*, 1460 *days* (4 *years*) respectively. The CPC (gauges) and ECMWF 3 hourly and TRMM results are shown as flat reference lines. (For interpretation of the references to colour in this figure legend, the reader is referred to the web version of this article.)

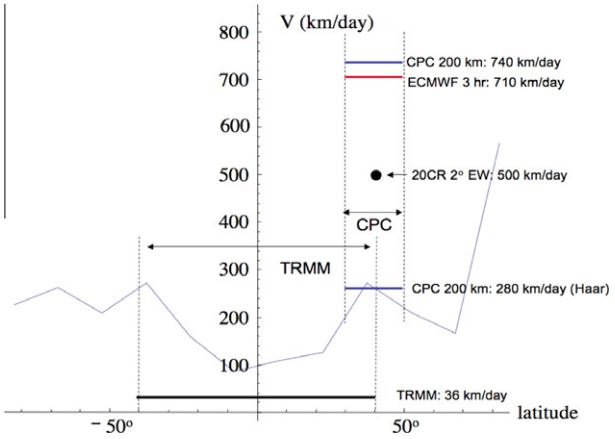

Fig. 8c. This shows the effective speeds obtained as the ratios of the spatial to temporal outer scales for the data in Figs. 8a and 8b.

ilar although due to the larger Δt available, we see hints that $\tau_c \approx 30$ years after which the fluctuations begin to increase again. One of the advantages of the Haar wavelet over other techniques such as the Detrended Fluctuation Analysis (DFA, see e.g. [46]) technique is that the magnitudes of the fluctuations can be readily interpreted in terms of differences (when $H > 0$), or tendencies (when $H < 0$, i.e. the mean of the fluctuations averaged over Δt), these are indicated on the vertical axis in the figure.

To make the case for the existence of long range correlations (i.e. nontrivial scaling) even stronger, we can take the ratio of the mean (absolute) fluctuation to the RMS fluctuation. Theoretically, since $\xi(q) = qH - K(q)$, this ratio scales as $\Delta t^{K(2)/2}$ so that the result directly shows the deviations from Gaussianity. In addition, for universal multifractals $K(q) = C_1(q^\alpha - q)/(\alpha - 1)$ so that for $\alpha \approx 2$, $K(2)/2 \approx C_1$ hence the exponent $K(2)/2$ is a straightforward measure of the intermittency. The result is shown in Fig. 7b; although the low frequency weather regime has a low intermittency, it is non negligible right through to the limits of the CPC data. This is consistent with the significant trace moments even at fairly large Δt in Fig. 5. A summary of the regression exponents is given in Table 3. For comparison, the meteorological state variables typically have β_{lw} in the range ≈0.2 to ≈0.4 [63] so that we conclude that in the low frequency weather regime there are long range statistical dependencies so that precipitation is much like the other meteorological variables only with somewhat larger intermittency (C_1).

4. The latitudinal dependence of the precipitation cascade

Up until now we have tacitly assumed that the fundamental precipitation exponents were the same all over the globe. In order to study possible regional variations (which might also help illuminate some of the observed variations in the exponents from different study regions), it is useful to examine the latitudinal dependences. The CPC network is confined to too narrow a latitudinal band (30–50°N) to make such a study worthwhile. Similarly, the TRMM data is primarily tropical in character; we therefore considered the latitudinal dependence of the ECMWF interim reanalysis product which is global. In order to get good statistics with seasonal variations largely averaged out, we used the daily ECMWF stratiform precipitation products for the four years 2005–2008, using 15° wide latitude bands. Fig. 8a shows the zonal and temporal C_1 variations; unsurprisingly we see that there is high degree of north and south symmetry. In addition, the high latitudes have the lowest intermittency (C_1) and the tropics the highest although there appears to be a dip near the equator which has no obvious explanation. Space and time values are extremely close to each other supporting the idea that at the level of the exponents, that horizontal space and time are isotropic (there can still be a "trivial" anisotropy i.e. "squashing" of structures that is independent of scale). Mirroring this variation in C_1 is the variation in the spatial and temporal outer scales (Fig. 8b). We see that (with the exception of the TRMM temporal outer scale) that there is more agreement between the different analyses and the ECMWF interim outer scales than with the C_1 estimates; in space the latter are within about ±50% of 30,000 km. We see that the temporal outer scale varies in nearly the same way.

The ratio of the spatial and temporal outer scales defines a space–time transformation speed (Fig. 8c). If the horizontal and spatial cascade structures are the same (the same $K(q)$ functions), then this corresponds to a unique mean advection speed (i.e. independent of scale λ, independent of intensity, q). In addition we notice that with the exception of the extreme high latitudes (where the product is unreliable), the speed is pretty much independent of latitude (about 200 km/day, close to that deduced for the CPC data from the Haar wavelets in Fig. 7a). For the ECMWF products, the $K(q)$ for time and space are indeed very similar (Fig. 6b, similar C_1 values), so that the result has this broad interpretation. However, as can be seen from the comparison with the CPC and TRMM results, the mean CPC and TRMM results are quite different (larger and smaller respectively). This is perhaps not surprising since from either the $K(q)$ curves (Fig. 6a, 6c) or the zonal space versus temporal C_1 values (Table 2), we see that the velocity does depend somewhat on scale and on intensity (implicitly since the ratio of the corresponding spatial and temporal $K(q)$'s depends somewhat on q), and at the time of writing it is not clear if this effect is real or is an artefact of the techniques for estimating areal precipitation.

5. Conclusions

5.1. Discussion

There is now a large body of empirical evidence indicating that the basic cascade framework is indeed appropriate for precipitation. Surprisingly, applications of cascades to the atmosphere – including to precipitation – have been largely confined to studies at scales smaller than ≈500–1000 km and most often to time scales less than a few days. However, the development of readily accessible global scale data sets makes it now possible to extend cascade analyses up to planetary spatial scales and centennial time scales. In this paper, we performed an inter-comparison of four rather different global (or near global) precipitation data sets: satellite radar, gridded in situ gauge series, and precipitation fields from reanalyses. Overall, the four data sets spanned the range of scales from hours to 138 years, from 4.3 km to planetary scales (in both east–west and north south directions).

All eleven analyses – three data sets analysed in each of three directions x, y, and t and a fourth in x and t only – showed very good scaling and clear evidence of global scale cascades over all the accessible spatial scales and in time out to about 5 days with effective outer cascade time scales being somewhat larger. Indeed although there are some deviations from scaling at the smallest spatial scales these were mostly for the lowest order moments which are sensitive to low and zero rain rate measurement issues and to the highest moments which are sensitive to problems in estimating the high rain rates. It is significant that the deviations from log–log linearity of the individual products is of the order of a few percent whereas the differences from product to product in the logarithm of the $q = 2$ moments can be as large as ≈100%. It is hard to avoid the conclusion that instrumental limitations are considerable.

This analysis shows that rain is qualitatively like the conventional meteorological state variables (in particular, the wind, temperature, humidity, geopotential height) in having planetary scale cascades in space and in time up to scales corresponding to the lifetime of planetary structures: the transition from weather to low frequency weather at $\tau_w \approx 5$–10 days. However, a significant difference with the state variables is that the intermittency – whether characterised by the whole exponent function $K(q)$ or by its derivative $C_1 = K'(1)$ – is much larger than for the usual meteorological variables (≈0.3–0.4 rather than 0.05–0.1 although it is close to the $C_1 \approx 0.5$ of the turbulent energy flux), so that the multifractal intermittency of rain is of more central importance than for the other state variables. While our qualitative conclusions about the existence of planetary scale cascades seem robust, there are still unexplained differences in the parameters; differences between products and differences depending on the direction of the analysis (i.e. x, y, or t). For a single product, differences in direction imply a scaling anisotropy whereas for a given direction, the differences between products imply that the different precipitation data sets are not fully compatible with each other. In the case of possi-

ble anisotropy, we argued that the data were probably compatible with equal exponents in the different directions whereas, the differences between data sets have still to be understood and have implications for the various methods of estimating space–time rainfall.

The exponents discussed above are large (roughly global) scale averages; how representative are these of real rain – are there significant regional variations? The ECMWF reanalyses were particularly convenient for answering this question; we examined the latitudinal variation of the cascades (in the zonal direction and time). Significantly, although the spatial and temporal C_1 values and external scales varied somewhat, they remained highly correlated so that it seems that the latitudinal variations of C_1 are important but that the cascade process remains isotropic in space–time. For example, in the tropics the C_1 values were $\approx$0.3–0.4 whereas at high latitudes they were $\approx$0.2–0.25. The velocity connecting space and time was relative constant at about 200 km/day. In this regard the rain field is again similar to the other meteorological fields; see the study of latitudinal variations in reanalysis state variables in [43].

5.2. Implications for precipitation

The marriage of turbulence and precipitation science that began nearly 25 years ago has stimulated several important developments in cascade processes and has resulted in numerous applications throughout atmospheric science and hydrology. However, applying cascade processes to precipitation raises many fundamental issues several of which are addressed by the analyses presented here. These theoretical issues include (a) the relation of the rain rate field to the scale by scale precipitation "flux" field: what is the value of H; is it zero or nonzero? (b) the nature of the scale by scale cascade conservation: is it microcanonical or canonical? (c) the question of universality: is it weak (log Poisson) or strong (log Levy)... or none at all? (d) the nature of the low and zero rain rates: is the rain process on a fractal support or is there a low threshold below which the values are effectively truncated to zero? (e) what is the nature of the extremes: are they classical (thin or long tailed) or are they power laws? (is q_D infinite or finite?), finally, (f) are there long-range statistical dependencies at monthly, yearly and longer scales or do the precipitation statistics tend to Gaussian white noises? In the case of point (a) we used the huge CPC gauge data set to provide the estimates $H \approx 0.17 \pm 0.11$, (i.e. H is apparently not zero) and in the case of point (e), we found $q_D \approx 3$: if true the latter would rule out microcanonical models (point b) and make log Poisson models (point c) implausible. To answer point (f) we used spectra and Haar wavelets to show that there are indeed long range dependencies even beyond 20 year scales.

At a more practical level, our results imply that there is still much work to be done in measuring space–time rainfall: the statistical differences between the various precipitation products is large enough so that at most only one of the products could be "correct", it is more likely they all suffer from various systematic deficiencies. Indeed, the scale by scale, intensity by intensity product inter comparisons show that the relatively large deviations from log–log linearity (i.e. from the scaling symmetry) are more likely to be due to instrumental effects, so that it is premature to conclude that the scaling symmetry itself breaks down until $\tau_w \approx$ 5–10 days in time or below planetary scales in space. Concretely, for the radar and gauges, the most obvious difficulties are in accurately estimating low and high rain rates, in the former of converting from effective reflectivity factors to rain rates and in the latter in estimating areal rainrate fields from (possibly sparse, fractal) networks of gauges. In all cases, the use of explicit space–time multifractal models are likely to continue to be indispensable tools in attempting to tame the huge intermittency of rain and understanding the deficiencies in the various measurement techniques. Similarly, the issue of whether $H = 0$ or otherwise and the nature of the low and zero rain rates is important in disaggregating rain at higher resolutions.

Acknowledgement

J. Pinel acknowledges a Quebec FQRNT scholarship.

References

[1] Hurst HE. Long-term storage capacity of reservoirs. Trans Am Soc Civil Eng 1951;116:770.
[2] Mandelbrot BB, Wallis JR. Noah, Joseph and operational hydrology. Water Resour Res 1968;4:909.
[3] Lovejoy S. Area perimeter relations for rain and cloud areas. Science 1982;187:1035.
[4] Lovejoy S, Schertzer D. Multifractals and rain. In: Kunzewicz ZW, editor. New uncertainty concepts in hydrology and water ressources. Cambridge University Press; 1995. p. 62–103.
[5] Lovejoy S, Schertzer D. Turbulence, rain drops and the $l^{1/2}$ number density law. New J Phys 2008;10(075017):32.
[6] Lovejoy S, Schertzer D, Allaire V. The remarkable wide range scaling of TRMM precipitation. Atmos Res 2008. http://dx.doi.org/10.1016/j.atmosres.2008.02.016.
[7] Olsson J, Berndtsson R. Temporal rainfall disaggregation based on scaling properties. Water Sci Technol 1998;37:73.
[8] Güntner A, Olsson J, Calver A, Gannon B. Cascade-based disaggregation of continuous rainfall time series: the influence of climate. Hydrol Earth Syst Sci 2001;5:145.
[9] Veneziano D, Iacobellis V. Multiscaling pulse representation of temporal rainfall. Water Resour Res 2002;38.
[10] Paulson KS, Baxter PD. Downscaling of rain gauge time series by multiplicative beta cascade. J Geophys Res 2007:112.
[11] Rupp DE, Keim RF, Ossiander M, Brugnach M, Selker JS. Time scale and intensity dependency in multiplicative cascades for temporal rainfall disaggregation. Water Resour Res 2009;45.
[12] Tessier Y, Lovejoy S, Hubert P, Schertzer D, Pecknold S. Multifractal analysis and modeling of rainfall and river flows and scaling, causal transfer functions. J Geophys Res 1996;31D:26.
[13] De Lima I. Multifractals and the temporal structure of rainfall PhD thesis, Wageningen; 1998.
[14] De Lima I, Grasman J. Multifractal analysis of 15-min and daily rainfall from a semi-arid region in Portugal. J Hydrol 1999;220:1.
[15] Garcia-Marin AP, Jimenez-Hornero FJ, Ayuso-Munoz JL. Universal multifractal description of an hourly rainfall time series from a location in southern Spain. Atmosfera 2008;21:347.
[16] Serinaldi F. Multifractality, imperfect scaling and hydrological properties of rainfall time series simulated by continuous universal multifractal and discrete random cascade models. Nonlinear Proc Geophys 2010;17:697.
[17] de Montera L, Barthès L, Mallet C, Golé P. Rain universal multifractal parameters revisited with dual-beam spectropluviometer measurements. J Hydrometeorol 2009;10:493.
[18] Verrier S, De Montera L, Barthès L, Mallet C. Multifractal analysis of African monsoon rain fields, taking into account the zero rain-rate problem. J Hydrol 2010;389:111.
[19] Schertzer D, Lovejoy S. Physical modeling and analysis of rain and clouds by anisotropic scaling of multiplicative processes. J Geophys Res 1987;92:9693.
[20] Gupta VK, Waymire E. A statistical analysis of mesoscale rainfall as a random cascade. J Appl Meteorol 1993;32:251.
[21] Schertzer D, Lovejoy S. Universal multifractals do exist. J Appl Meteorol 1997;36:1296.
[22] Deidda R, Benzi R, Siccardi F. Multifractal modeling of anomalous scaling laws in rainfall. Water Resour Res 1999;35:1853.
[23] Onof C, Arnbjerg-Nielsen K. Quantification of anticipated future changes in high resolution design rainfall for urban areas. Atmos Res 2009;92:350.
[24] Wang L, Onof C, Maksimovic C. Reconstruction of sub-daily rainfall sequences using multinomial multiplicative cascades. Hydrol Earth Syst Sci Discuss 2010;7:5267.
[25] Olsson J, Niemczynowicz J. Multifractal analysis of daily spatial rainfall distributions. J Hydrol 1996;187:29.
[26] Olsson J. Evaluation of a scaling cascade model for temporal rain-fall disaggregation. Hydrol Earth Syst Sci 1998;2:19.
[27] Pathirana A, Herath S, Yamada T. Estimating rainfall distributions at high temporal resolutions using a multifractal model. Hydrol Earth Syst Sci 2003;7:668.
[28] Veneziano D, Furcolo P, Iacobellis V. Imperfect scaling oftime and spacetime rainfall. J Hydrol 2006;322:105.
[29] Sun X, Barros AP. An evaluation of the statistics of rainfall extremes in rain gauge observations and satellite-based and reanalysis products using universal multifractals. J Hydrometeorol 2010;11:388.

[30] Hoang CT, Tchiguirinskaia I, Schertzer D, Arnaud P, Lavabre J, Lovejoy S. Assessing the high frequency quality of long rainfall series. J Hydrol 2012. http://dx.doi.org/10.1016/j.jhydrol.2012.01.044.
[31] Over TM, Gupta VK. Statistical analysis of Mesoscale rainfall: dependence of a random cascade generator on large-scale forcing. J Appl Meteorol 1994;33:1526.
[32] Over T, Gupta VK. A space-time theory of mesoscale rainfall using random cascades. J Geophys Res 1996;101:26319.
[33] Pathirana A, Herath S. Multifractal modelling and simulation of rain fields exhibiting spatial heterogeneity. Hydrol Earth Syst Sci 2002;6:695.
[34] Cahalan R. Bounded cascade clouds: albedo and effective thickness. Nonlin Proc Geophys 1994;1:156.
[35] Marshak A, Davis A, Cahalan RF, Wiscombe WJ. Bounded cascade models as nonstationary multifractals. Phys Rev E 1994;49:55.
[36] Menabde M, Harris D, Seed A, Austin G, Stow D. Multiscaling properties of rainfall and bounded random cascades. Water Resour Res 1997;33:2823.
[37] Lovejoy S, Schertzer D. Multifractals, cloud radiances and rain. J Hydrol 2006;322:59–88. http://dx.doi.org/10.1016/j.hydrol.2005.02.042.
[38] Carsteanu A, Foufoula-Georgiou E. Assessing dependence among the weights in a mulitplicative cascade model of temporal rainfall. J Geophys Res 1996;101:26363.
[39] Lovejoy S. Why the bare/dressed cascade distinction matters: interactive comment on "Reconstruction of sub-daily rainfall sequences using multinomial multiplicative cascades" by L. Wang et al. Hydrol Earth Syst Sci Discuss 2010;7(C1).
[40] Tessier Y, Lovejoy S, Schertzer D. Universal multifractals: theory and observations for rain and clouds. J Appl Meteorol 1993;32:223.
[41] Stolle J, Lovejoy S, Schertzer D. The stochastic cascade structure of deterministic numerical models of the atmosphere. Nonlinear Proc Geophys 2009;16:1.
[42] Lovejoy S, Schertzer D. Towards a new synthesis for atmospheric dynamics: space–time cascades. Atmos Res 2010;96:1.
[43] Lovejoy S, Schertzer D. Space-time cascades and the scaling of ECMWF reanalyses: fluxes and fields. J Geophys Res 2011;116.
[44] Lovejoy S, Tuck AF, Schertzer D. The Horizontal cascade structure of atmospheric fields determined from aircraft data. J Geophys Res 2010;115:D13105.
[45] Lovejoy S et al. Atmospheric complexity or scale by scale simplicity? Geophys Res Lett 2009;36:L01801.
[46] Kantelhardt JW et al. Long-term persistence and multifractality of precipitation and river runoff record. J Geophys Res 2006;111.
[47] Compo GP, Whitaker JS, Sardeshmukh PD, Matsui N, Allan RJ, Yin X, et al. The Twentieth Century reanalysis project. Quart J R Meteorol Soc 2011;137:1.
[48] Team TPR. "Tropical Rainfall Measuring Mission, TRMM, Precipitation Radar Algorithm, Instruction Manual For Version 6 (Japan Aerospace Exploration Agency (JAXA), National Aeronautics and Space Administration (NASA); 2005).
[49] Lovejoy S, Schertzer D. The weather and climate: emergent laws and multifractal cascades, Cambridge University Press, Cambridge; in press. p. 500.
[50] Lilley M, Lovejoy S, Desaulniers-Soucy N, Schertzer D. Multifractal large number of drops limit in Rain. J Hydrol 2006;328:20.
[51] Hubert P, Biaou A, Schertzer D. De la Meso-Echelle à la Micro-Echelle: Desagregation/Agregation Multifractale et Spatio-Temporelle des Precipitations. Report, Armines-EdF; 2002.
[52] Lovejoy S, Tuck AF, Schertzer D, Hovde SJ. Reinterpreting aircraft measurements in anisotropic scaling turbulence. Atmos Chem Phys 2009;9:1.
[53] Lovejoy S, Schertzer D. Scale invariance in climatological temperatures and the spectral plateau. Ann Geophys 1986;4B:401.
[54] Ladoy P, Schmitt F, Schertzer D, Lovejoy S. Variabilité temporelle des observations pluviométriques à Nimes. C R Acad Sci 1993;317(II):775.
[55] Olsson J. Limits and characteristics of the multifractal behavior of a high-resolution rainfall time series. Non-linear Processes Geophys 1995;2:23.
[56] Kiely G, Ivanova K. Multifractal analysis of hourly precipitation. Phys Chem Earth Pt B 1999;24:781.
[57] Schertzer D, Tchiguirinskaia I, Lovejoy S, Hubert P. No monsters, no miracles: in nonlinear sciences: hydrology is not an outlier. Hydro Sciences J 2010;55:965. http://dx.doi.org/10.1080/02626667.2010.505173.
[58] Schertzer D, Veyssere JM, Hallegate S, Hubert P, Bendjoudi H, Lovejoy S. Hydrological Extremes and Multifractals: from GEV to MEV?
[59] Lovejoy S, Schertzer D. Paper presented at the Cloud conference, Madison, Wi.; July 12–14 2006.
[60] Lovejoy S, Schertzer D. Low frequency weather and the emergence of the Climate. In: Sharma AS, Bunde A, Baker D, Dimri VP, editors. Complexity and Extreme Events in Geosciences, AGU monographs; in press.
[61] Hubert P, Tessier Y, Ladoy P, Lovejoy S, Schertzer D, Carbonnel JP, et al. Multifractals and extreme rainfall events. Geophys Res Lett 1993;20:931.
[62] Harris D, Menabde M, Seed A, Austin G. Multifractal characterization of rain fields with a strong orographics influence. J. Geophys. Res. 1996;101:26405.
[63] Kantelhardt JW, Zscchegner SA, Koscielny-Bunde K, Havlin S, Bunde A, Stanley HE, et al. Multifractal detrended fluctuation analysis of nonstationary time series. Physica A 2002;316:87.